

A machine learning augmented density functional theory investigation of hydrogen adsorption on defective nitrogen doped carbon nanotubes

Rasmus Kronberg, Heikki Lappalainen, and Kari Laasonen*

*Research Group of Computational Chemistry, Department of Chemistry and Materials Science, Aalto University,
P.O. Box 16100, FI-00076 Aalto, Finland*

E-mail: kari.laasonen@aalto.fi

Abstract

1 Introduction

2 Theoretical Methods

2.1 Model Systems

Hydrogen adsorption was studied on 16 different nitrogen doped and defective CNTs, each consisting of 224 atoms in a periodically repeated simulation cell with dimensions of approximately $3.1 \times 3.1 \times 1.7 \text{ nm}^3$. Two different CNT types were considered, namely the achiral zigzag (14, 0) and armchair (8, 8) CNTs, both having experimentally realistic diameters of roughly 1.1 nm. Thus, roughly 2.0 nm of vacuum was applied to decouple periodically repeated images of the systems in the xy -plane. Of the various dopant configurations, two substitutional graphitic, three pyridinic and three pyrrolic nitrogen moieties were explored with single vacancy, double vacancy and Stone–Wales rotation type defects, resulting in dopant and vacancy concentrations ranging between 0.4–1.8 at% and 0–0.9 at%, respectively. The dopant and defect types were selected based on previous experimental and computational studies^{1–6} on probable doping configurations in CNTs. The investigated NCNT substrates are summarized in Table 1.

Given the defined reference configurations, the hydrogen affinity was probed considering all possible sites in the positive half-space containing the nitrogen/defect configuration. Adsorption sites on the other side of the nanotubes were excluded. Having determined the most stable adsorption site for each nanotube, the minimum energy adsorbed systems were selected as substrates for a second round of adsorption energy calculations, thus now including two hydrogen adsorbates. This procedure was repeated for the cases of three and finally four adsorbed hydrogen intermediates to assess the impact of hydrogen coverage.

2.2 Electronic Structure Calculations

Spin-polarized density functional theory calculations were carried out using the hybrid Gaussian and plane waves (GPW) method⁷ as implemented in the CP2K/QUICKSTEP electronic structure and molecular dynamics software package^{8–10}. The plane wave expansion of the electron density was truncated at an optimized cutoff value of 600 Ry while the orbital functions of the valence electrons were

expanded in short-range, molecularly optimized and polarized double- ζ Gaussian basis sets (MOLOPT-SR-DZVP)¹¹. Remaining ionic cores were represented by correspondingly adapted dual-space norm-conserving Goedecker–Teter–Hutter (GTH) pseudopotentials^{12–14}.

The exchange-correlation energy was described using the Perdew–Burke–Ernzerhof (PBE) generalized gradient approximation (GGA) including dispersion corrections based on the DFT-D3 scheme of Grimme *et al.*¹⁵ with rational Becke–Johnson damping¹⁶. Direct minimization of the electronic Kohn–Sham energy functional was conducted by the orbital transformation (OT) method¹⁷ employing an energy convergence threshold of 2.7×10^{-5} eV. Geometries were optimized by relaxing the atomic positions using the Broyden–Fletcher–Goldfarb–Shanno (BFGS) algorithm until the force on any atom was less than 2.3×10^{-2} eV Å^{−1}. Net atomic charges and spin moments were calculated self-consistently from the optimized electron density using the iterative Hirshfeld partitioning procedure (Hirshfeld-I)¹⁸. This population analysis scheme enables a rational selection of the promolecule and has been shown to compare favorably with alternative population analyses based on the electrostatic potential or topological partitioning^{19–21}.

Hybrid Hartree–Fock/DFT (HF/DFT) calculations were performed on geometries relaxed at the PBE level of theory using the truncated, long-range corrected PBE0²² functional (PBE0-TC-LRC) introduced by Guidon *et al.*²³ in which the standard $1/r$ Hartree–Fock exchange (HFX) term is truncated using a cutoff radius of 8 Å. The auxiliary density matrix method (ADMM)²⁴ was further applied to reduce the cost of computing the exact HFX energy. In this approach, an auxiliary pFIT3 basis set was used to project the original density matrix into an auxiliary one for which the HFX energy can be computed more efficiently, facilitating hybrid HF/DFT calculations of fairly large systems.

2.3 Random Forests Ensemble Learning

Random forests (RF) is a machine learning technique that operates by generating an ensemble of decision trees based on training data composed of several features for each sample and outputting the mean prediction of the individual estimators for a target quantity²⁵. In order to reduce correlation between individual trees, the random subspace method is applied during tree generation such that only a stochastically chosen subset of all input features is considered when splitting each node. A second level

Table 1: Specification and illustration of the studied model NCNT systems. The abbreviations V₁, V₂ and SW denote a single vacancy, double vacancy and Stone–Wales rotation, respectively. For the Stone–Wales defect two distinct nitrogen positions resembling indole (N_{1a}) and indolizine (N_{1b}) structures were considered.

| N moiety | Defect | (n, m) | Image |
|---------------------------|----------------|-------------------|-------|
| Graphitic, N ₁ | None | (14, 0) (8, 8) | |
| Graphitic, N ₂ | None | (14, 0) (8, 8) | |
| Pyridinic, N ₁ | V ₁ | (14, 0) (8, 8) | |
| Pyridinic, N ₃ | V ₁ | (14, 0) (8, 8) | |
| Pyridinic, N ₄ | V ₂ | (14, 0) (8, 8) | |
| Pyrrolic, N ₁ | V ₁ | (14, 0) (8, 8) | |
| Pyrrolic, N _{1a} | SW | (14, 0) (8, 8) | |
| Pyrrolic, N _{1b} | SW | (14, 0) (8, 8) | |

of randomness is injected by using a bootstrap sample of the training data for each tree, *i.e.* training samples are selected with replacement so that each object may be chosen a variable amount of times. On average, $1/e \approx 37\%$ of the training samples will not be used for the construction of a given tree, forming the “out-of-bag” (OOB) set of samples, which may be used for internal validation. By training a

random forest of stochastically distinct decision trees, both numerical (regression) and categorical (classification) target variables of unseen test data can be predicted robustly with reduced overfitting compared to conventional decision trees or *e.g.* artificial neural networks (ANN)²⁶.

For the purpose of exploring how strongly and in what manner different features of defective NCNTs contribute to the inherent hydrogen adsorption properties, we trained a random forest algorithm using the scikit-learn²⁷ Python package for the regression task of predicting the adsorption energy ΔE using a dataset of 6400 adsorption configurations. A forest of 200 trees was chosen and when splitting each node during the construction of a tree the best split was determined using a subset of 10 from the full input randomly selected features. In total 25 different features were considered, detailed in Table X. 90% of the full, randomized dataset was used for training while 10% was left for performance testing. Due to the heterogeneity of the dataset, the train-test split was stratified by the adsorption energies in order to obtain representative training and test sets. 10-fold cross-validation was furthermore applied to improve the reliability of the predictions on the held-out samples.

Estimating feature importances is a delicate matter. By default, the scikit-learn random forest implementation calculates feature importances based on the mean decrease in impurity (MDI). An impurity measure $i(t)$ is a figure of merit of any node t such that the smaller the impurity, the purer the node is. With the full training set initially represented by a single node, successive binary splits s_t that maximize the decrease in impurity are made, partitioning the data into increasingly homogeneous groups until the terminal nodes (leaves) cannot be made any purer. Denoting the impurity decrease as $\Delta i(s_t, t)$, the importance of a certain feature j for predicting the target variable is then defined as the sum of weighted impurity decreases for all nodes where j is used, averaged over all trees $\{f_m\}_{m=1}^M$ in the random forest^{28,29},

$$I_j^{\text{MDI}} = \frac{1}{M} \sum_{m=1}^M \sum_{t \in f_m} w(t) \Delta i(s_t, t | j), \quad (1)$$

where the weight $w(t)$ is the fraction of samples reaching node t . Thus, features used at the top of a decision tree contribute to the final prediction of a larger portion of the input samples, and Eq. (1) corresponds consequently to a normalized feature importance estimate accounting for the expected fraction of the samples feature j contributes to in combination with the decrease in impurity gained upon splitting them. One of the most common impurity measures is the Gini index³⁰, and when employed Eq. (1) is also known as the Gini importance. A further overview of the different flavors of impurity measures is, however, beyond the scope of the present brief discussion.

Unfortunately, impurity based feature importances suffer from a major drawback as they tend to inflate the importances of high cardinality numerical features, *i.e.* variables that may attain a broad spectrum of unique values in contrast to *e.g.* binary or finite categorical features^{29,31}. This bias towards continuous high cardinality features arises from their inherent ability to offer more potential cut-points that may by chance produce a large impurity decrease when the node is split. Consequently, even randomly generated numbers can be ranked misleadingly as highly important, resulting in severe inconsistencies in feature attributions.

An effective mitigation to this issue has been recently

Table 2: Mathematical formulation and explanation of all 25 input features used in the RF model. A glossary of abbreviations and auxiliary parameters used for defining each feature is presented in Table X in the Supporting Information.

| Feature | Definition | Unit | Explanation |
|-----------------------|---|------|---|
| x_k | $N_k/N_{\text{CNT}} \times 100\%$ | at% | Atomic concentration ($k = \text{N, V, H}$) |
| $\min\{d_k\}$ | $\min \left\{ \sqrt{(r\theta_k)^2 + z_k^2} \right\}$ | Å | Shortest curvilinear distance between two atoms ($k = \text{NS, HS}$) |
| $\langle d_k \rangle$ | $\left\langle \sqrt{(r\theta_k)^2 + z_k^2} \right\rangle$ | Å | Average curvilinear distance between two atoms ($k = \text{NS, HS}$) |
| RMSD | $\sqrt{\langle (\Delta\mathbf{R})^2 \rangle}$ | Å | Adsorption-induced root-mean-squared displacement of atomic positions |
| RmaxSD | $\sqrt{\max \{(\Delta\mathbf{R})^2\}}$ | Å | Adsorption-induced root-maximum-squared displacement of atomic positions |
| χ | $\arctan \left(\frac{\sqrt{3}m}{2n+m} \right)$ | rad | Chiral angle of (n, m) CNT |
| $\min\{\varphi_k\}$ | $\min \{\arccos(\hat{\mathbf{u}}_k \cdot \hat{\mathbf{v}}_k)\}$ | rad | Smallest angle formed by adjacent atoms where the vertex is defined by atom k ($k = \text{N, S}$) |
| $\max\{\varphi_k\}$ | $\max \{\arccos(\hat{\mathbf{u}}_k \cdot \hat{\mathbf{v}}_k)\}$ | rad | Largest angle formed by adjacent atoms where the vertex is defined by atom k ($k = \text{N, S}$) |
| α_k | $\arccos(\hat{\mathbf{w}}_k \cdot \hat{\mathbf{e}}_z)$ | rad | Angular displacement of the adsorption site wrt. the closest atom of kind k ($k = \text{N, H}$) |
| CN_k | | – | Coordination number of atom k ($k = \text{N, S}$) |
| ΔCN_k | | – | Adsorption-induced change in CN_k |
| Z | | – | Atomic number of the adsorption site |
| M | $2S + 1$ | – | Spin multiplicity of the system |
| q | $n_{\text{val}} - (n_{\uparrow} + n_{\downarrow})$ | e | Residual charge on the adsorption site |
| μ | $n_{\uparrow} - n_{\downarrow}$ | e | Spin polarization on the adsorption site |
| E_g | $E_{\text{LUMO}} - E_{\text{HOMO}}$ | eV | Energy gap, for open-shell systems the SOMO-LUMO gap |

presented by Lundberg and Lee³² and is based on so called Shapley values known from cooperative game theory³³. In simple terms, Shapley values measure the contribution of each member of a coalition in a collaborative game, providing a theoretically well-founded division of the generated surplus among the members based on the average of all contributions made by an individual. In the context of machine learning, each feature represents a single player of a coalition of features that cooperate towards forming a prediction and the contribution of each player are the feature importances, the Shapley values. To calculate the Shapley value of a feature j , one considers a subset S of all features F and trains a general model f both with the feature j present in the subset $(S \cup \{j\})$ and with the feature absent (S). The marginal contribution of the feature in a specific coalition is then $f(S \cup \{j\}) - f(S)$ and averaging over all possible permutations in which a coalition S can be formed yields the Shapley value ϕ_j as

$$\phi_j = \sum_{S \subseteq F \setminus \{j\}} \frac{|S|!(|F| - |S| - 1)!}{|F|!} [f(S \cup \{j\}) - f(S)], \quad (2)$$

where $|\cdot|$ denotes the number of elements in a set. The Shapley values satisfy three important properties of feature attribution methods: local accuracy, missingness and consistency³². Local accuracy, or additivity, entails that the

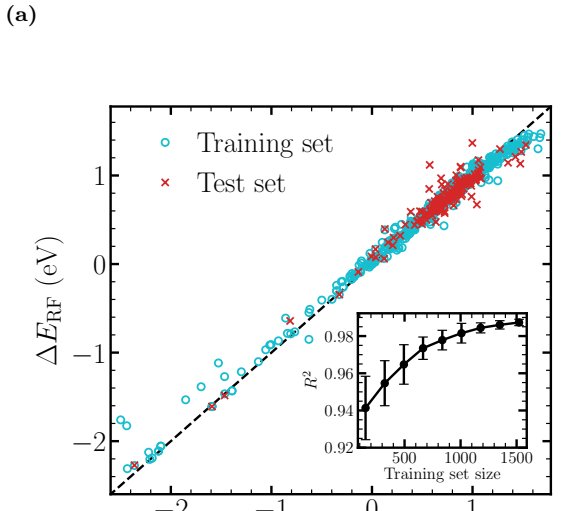
sum of the individual feature contributions equals the model output, while missingness requires that features absent in the original input, *i.e.* $f(S \cup \{j\}) = f(S)$, have no attributed impact ($\phi_j = 0$). Perhaps most importantly, consistency ensures that if a model changes such that some feature's contribution *increases*, the importance of this feature does not *decrease*. The requirement of consistency is not satisfied by previous feature importance evaluation methods based on standard concepts such as the MDI³⁴. This is the main advantage of using Shapley values for feature attribution, enabling reliable and meaningful comparisons across the feature space.

To estimate feature importances based on Shapley values, we apply the concept of Shapley additive explanations (SHAP) as implemented in the efficient `shap` Python package and optimized for tree ensemble methods (TreeSHAP)³⁴. The SHAP values are a special case of Eq. (2) in which the general set function $f(S)$ is defined as the expected output value of the machine learning model \hat{f} with input x given a subset S of the features, $\mathbb{E}[\hat{f}(x) | xs]$. As the SHAP values are local feature attributions in the sense that they calculate the contribution of each feature with respect to every observation i , the *global* SHAP importance of feature j is calculated as the mean magnitude of the individual SHAP values,

$$I_j^{\text{SHAP}} = \frac{1}{L} \sum_{i=1}^L |\phi_j^{(i)}|, \quad (3)$$

where L indicates the number of samples. Although SHAP values are a fairly recent feature attribution method, the concept has already been applied successively in the context of machine learning augmented computational chemistry for explaining model outputs for band gaps and exciton binding energies in 2D materials³⁵, exchange-correlation functional fitting³⁶ and compound activity prediction in medicinal chemistry³⁷.

3 Results and Discussion



(b)

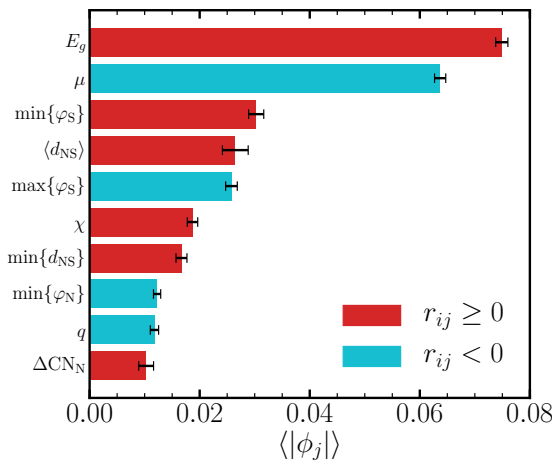


Figure 1

4 Conclusions

Acknowledgement R.K. acknowledges funding in the form of a doctoral scholarship by the School of Chemical Engineering of Aalto University. Computing resources were provided

by the Finnish IT Center for Science (CSC).

Supporting Information Available

References

- (1) Ayala, P.; Arenal, R.; Rümmeli, M.; Rubio, A.; Pichler, T. The doping of carbon nanotubes with nitrogen and their potential applications. *Carbon* **2010**, *48*, 575–586.
- (2) Susi, T.; Kotakoski, J.; Arenal, R.; Kurasch, S.; Jiang, H.; Skakalova, V.; Stephan, O.; Krasheninnikov, A. V.; Kauppinen, E. I.; Kaiser, U.; Meyer, J. C. Atomistic description of electron beam damage in nitrogen-doped graphene and single-walled carbon nanotubes. *ACS Nano* **2012**, *6*, 8837–8846.
- (3) Arenal, R.; March, K.; Ewels, C. P.; Rocquefelte, X.; Kociak, M.; Loiseau, A.; Stéphan, O. Atomic configuration of nitrogen-doped single-walled carbon nanotubes. *Nano Lett.* **2014**, *14*, 5509–5516.
- (4) Susi, T.; Pichler, T.; Ayala, P. X-ray photoelectron spectroscopy of graphitic carbon nanomaterials doped with heteroatoms. *Beilstein J. Nanotechnol.* **2015**, *6*, 177–192.
- (5) Davodi, F.; Tavakkoli, M.; Lahtinen, J.; Kallio, T. Straightforward synthesis of nitrogen-doped carbon nanotubes as highly active bifunctional electrocatalysts for full water splitting. *J. Catal.* **2017**, *353*, 19–27.
- (6) Murdachaew, G.; Laasonen, K. Oxygen evolution reaction on nitrogen-doped defective carbon nanotubes and graphene. *J. Phys. Chem. C* **2018**, *122*, 25882–25892.
- (7) Lippert, G.; Hutter, J.; Parrinello, M. A hybrid Gaussian and plane wave density functional scheme. *Mol. Phys.* **1997**, *92*, 477–488.
- (8) VandeVondele, J.; Krack, M.; Mohamed, F.; Parrinello, M.; Chassaing, T.; Hutter, J. Quickstep: Fast and accurate density functional calculations using a mixed Gaussian and plane waves approach. *Comput. Phys. Commun.* **2005**, *167*, 103–128.
- (9) Hutter, J.; Iannuzzi, M.; Schiffmann, F.; VandeVondele, J. CP2K: atomistic simulations of condensed matter systems. *Wiley Interdiscip. Rev.: Comput. Mol. Sci.* **2014**, *4*, 15–25.
- (10) Kühne, T. D.; Iannuzzi, M.; Del Ben, M.; Rybkin, V. V.; Seewald, P.; Stein, F.; Laino, T.; Khalilullin, R. Z.; Schütt, O.; Schiffmann, F.; Golze, D.; Wilhelm, J.; Chulkov, S.; Bani-Hashemian, M. H.; Weber, V.; Borštník, U.; Taillefumier, M.; Jakobovits, A. S.; Lazzaro, A.; Pabst, H.; Müller, T.; Schade, R.; Guidon, M.; Andermatt, S.; Holmberg, N.; Schenter, G. K.; Hehn, A.; Bussy, A.; Belleflamme, F.; Tabacchi, G.; Glöök, A.; Lass, M.; Bethune, I.; Mundy, C. J.; Plessl, C.; Watkins, M.; VandeVondele, J.; Krack, M.; Hutter, J. CP2K: An electronic structure and molecular dynamics software package-Quickstep: Efficient and accurate electronic structure calculations. *J. Chem. Phys.* **2020**, *152*, 194103.
- (11) VandeVondele, J.; Hutter, J. Gaussian basis sets for accurate calculations on molecular systems in gas and condensed phases. *J. Chem. Phys.* **2007**, *127*, 114105.
- (12) Goedecker, S.; Teter, M.; Hutter, J. Separable dual-space Gaussian pseudopotentials. *Phys. Rev. B* **1996**, *54*, 1703.
- (13) Hartwigsen, C.; Goedecker, S.; Hutter, J. Relativistic separable dual-space Gaussian pseudopotentials from H to Rn. *Phys. Rev. B* **1998**, *58*, 3641.
- (14) Krack, M. Pseudopotentials for H to Kr optimized for gradient-corrected exchange-correlation functionals. *Theor. Chem. Acc.* **2005**, *114*, 145–152.
- (15) Grimme, S.; Antony, J.; Ehrlich, S.; Krieg, H. A consistent and accurate ab initio parametrization of density functional dispersion correction (DFT-D) for the 94 elements H-Pu. *J. Chem. Phys.* **2010**, *132*, 154104.
- (16) Grimme, S.; Ehrlich, S.; Goerigk, L. Effect of the damping function in dispersion corrected density functional theory. *J. Comput. Chem.* **2011**, *32*, 1456–1465.
- (17) Weber, V.; VandeVondele, J.; Hutter, J.; Niklasson, A. M. Direct energy functional minimization under orthogonality constraints. *J. Chem. Phys.* **2008**, *128*, 084113.
- (18) Bultinck, P.; Van Alsenoy, C.; Ayers, P. W.; Carbó-Dorca, R.

- Critical analysis and extension of the Hirshfeld atoms in molecules. *J. Chem. Phys.* **2007**, *126*, 144111.
- (19) Bultinck, P.; Ayers, P. W.; Fias, S.; Tiels, K.; Van Alsenoy, C. Uniqueness and basis set dependence of iterative Hirshfeld charges. *Chem. Phys. Lett.* **2007**, *444*, 205–208.
 - (20) Van Damme, S.; Bultinck, P.; Fias, S. Electrostatic potentials from self-consistent Hirshfeld atomic charges. *J. Chem. Theory Comput.* **2009**, *5*, 334–340.
 - (21) Heidar-Zadeh, F.; Ayers, P. W.; Verstraelen, T.; Vinogradov, I.; Vöhringer-Martinez, E.; Bultinck, P. Information-theoretic approaches to atoms-in-molecules: Hirshfeld family of partitioning schemes. *J. Phys. Chem. A* **2017**, *122*, 4219–4245.
 - (22) Adamo, C.; Barone, V. Toward reliable density functional methods without adjustable parameters: The PBE0 model. *J. Chem. Phys.* **1999**, *110*, 6158–6170.
 - (23) Guidon, M.; Hutter, J.; VandeVondele, J. Robust periodic Hartree–Fock exchange for large-scale simulations using Gaussian basis sets. *J. Chem. Theory. Comput.* **2009**, *5*, 3010–3021.
 - (24) Guidon, M.; Hutter, J.; VandeVondele, J. Auxiliary density matrix methods for Hartree–Fock exchange calculations. *J. Chem. Theory. Comput.* **2010**, *6*, 2348–2364.
 - (25) Mitchell, J. B. Machine learning methods in chemoinformatics. *Wiley Interdiscip. Rev.: Comput. Mol. Sci.* **2014**, *4*, 468–481.
 - (26) Svetnik, V.; Liaw, A.; Tong, C.; Culberson, J. C.; Sheridan, R. P.; Feuston, B. P. Random forest: a classification and regression tool for compound classification and QSAR modeling. *J. Chem. Inf. Comput. Sci.* **2003**, *43*, 1947–1958.
 - (27) Pedregosa, F.; Varoquaux, G.; Gramfort, A.; Michel, V.; Thirion, B.; Grisel, O.; Blondel, M.; Prettenhofer, P.; Weiss, R.; Dubourg, V., et al. Scikit-learn: Machine learning in Python. *J. Mach. Learn. Res.* **2011**, *12*, 2825–2830.
 - (28) Breiman, L. Random forests. *Mach. Learn.* **2001**, *45*, 5–32.
 - (29) Louppe, G.; Wehenkel, L.; Sutera, A.; Geurts, P. Understanding variable importances in forests of randomized trees. *Adv. Neural Inf. Process Syst.* 2013; pp 431–439.
 - (30) Raileanu, L. E.; Stoffel, K. Theoretical comparison between the gini index and information gain criteria. *Ann. Math. Artif. Intell.* **2004**, *41*, 77–93.
 - (31) Strobl, C.; Boulesteix, A.-L.; Zeileis, A.; Hothorn, T. Bias in random forest variable importance measures: Illustrations, sources and a solution. *BMC Bioinform.* **2007**, *8*, 25.
 - (32) Lundberg, S. M.; Lee, S.-I. A unified approach to interpreting model predictions. *Adv. Neural Inf. Process Syst.* 2017; pp 4765–4774.
 - (33) Shapley, L. S. A value for n-person games. *Contributions to the Theory of Games* **1953**, *2*, 307–317.
 - (34) Lundberg, S. M.; Erion, G.; Chen, H.; DeGrave, A.; Prutkin, J. M.; Nair, B.; Katz, R.; Himmelfarb, J.; Bansal, N.; Lee, S.-I. From local explanations to global understanding with explainable AI for trees. *Nat. Mach. Intell.* **2020**, *2*, 2522–5839.
 - (35) Liang, J.; Zhu, X. Phillips-Inspired Machine Learning for Band Gap and Exciton Binding Energy Prediction. *J. Phys. Chem. Lett.* **2019**, *10*, 5640–5646.
 - (36) Mitrofanov, A.; Korolev, V.; Andreadi, N.; Petrov, V.; Kalmykov, S. Simple Automatized Tool for Exchange–Correlation Functional Fitting. *J. Phys. Chem. A* **2020**, *124*, 2700–2707.
 - (37) Rodríguez-Pérez, R.; Bajorath, J. Interpretation of Compound Activity Predictions from Complex Machine Learning Models Using Local Approximations and Shapley Values. *J. Med. Chem.* **2019**,

Graphical TOC Entry

